THERMAL ANALYSIS OF AN OCTAGONAL SHELL EARTH ORBITING BODY

Khalil M. Khalil
Mech, Eng. Dep.
College of Eng.
University of Baghdad
Baghdad- Iraq

Dr. Manhal M. Awda
Scientific Researcher
Al-Battany Space Research Comp.
Baghdad-Iraq

Dr. Ihsan Y. Hussain
Assistant Professor
Mech. Eng. Dept.
College of Eng./University Of Baghdad
Baghdad-Iraq

ABSTRACT

The thermal behavior of an octagonal shell orbiting body in space environments had been simulated theoretically in the present work, and a simplified experimental test in a thermal vacuum chamber was also made on half-scale model of the prototype to investigate the problem. A mathematical model was built and simulated numerically by using lumped system technique and finite difference control volume approach with explicit scheme. The body in its orbit around the earth is assumed to receive solar, albedo and earth radiation heat fluxes. The orbit is circular of (500-Km) height and (40^{o}) inclination. The developed computational algorithm is capable of calculating the heat fluxes on body faces and the temperature distribution of the body at any time instant. The results showed that the albedo and earth heat fluxes are smaller when the orbit is higher. In the side faces, the heat fluxes are maximum when orbit inclination is minimum, and vice versa, the inverse behavior is true for the upper and lower faces. The heat fluxes are maximum in winter solstice and minimum in summer solstice. If the difference between the emissivity and absorptivity values is low, the body reaches to synchronous steady state faster. The emissivity is affected more than absorptivity. The temperatures of faces, which see the earth, are more fluctuated than the other faces. Comparison between theoretical and experimental results showed good agreement.

الخلاصة

تم في هذا البحث دراسة التصرف الحراري لجسم ثماني مجوف يدور حول الأرض نظريا، مع إجراء دراسة عملية داخل حجرة حرارية مفرغة على نموذج بنصف أبعاد الطراز لدراسة المسالة. تم بناء نموذج رياضي تم حله عددياً باستخدام تقنية نظام الكتل و طريقة عددية هي الفروق المحددة لحجم محكوم. يستلم الجسم في مداره حول الأرض الفيض الحراري الشمسي ، الفيض الحراري المنعكس (البيدو) ، و الفيض الحراري الأرضي . المدار دائري الشكل ارتفاعه (500) كيلومتر ، و زاوية ميلان (40^{o}) درجة. النموذج الرياضي له القابلية على حساب الفيوض الحرارية على اوجه الجسم وتوزيع درجة الحرارة على الجسم عند أي لحظة زمنية. أظهرت النتائج أن الفيوض الحرارية الالبيدو والإشعاع الأرضي تقل عندما يزيد ارتفاع المدار . في السطوح الجانبية تكون الفيوض الحرارية أعلى ما يمكن عندما يكون الميل المداري اقل ما يمكن،والعكس بالعكس، وعكس هذا التصرف يحدث في السطحين العلوي و السفلي. الفيوض الحرارية أعلى

ما يمكن في الانقلاب الشتوي وأقل ما يمكن في الانقلاب الصيفي.إذا كان الفرق بين قيمة الأنبعاثية وقيمة الامتصاصية قليل يصل الجسم إلى حالة الاستقرار المتزامن بوقت أسرع. الأنبعاثية اكثر تأثير من الامتصاصية في التصرف الحراري للجسم. درجات الحرارة في الأوجه التي ترى الأرض أكثر تقلباً من بقية الاوجة . أظهرت المقارنة بين النتائج النظرية و العملية توافقاً جيداً.

KEY WORDS
Earth Orbiting Body, Octagonal, Thermal Analysis

INTRODUCTION

Satellite thermal design is now an essential engineering activity in the development of all space vehicles. Satellite thermal analysis is the first step in the thermal design, while thermal control is the second step. There are several sources of thermal energy acting on a satellite. For near-earth orbits the major external energy sources are solar radiation, earth-emitted radiation, and earth albedo radiation. . Internal heat dissipation is another source of heat load acting on satellite. The aerodynamic heating acts on the satellite in addition to the above mentioned sources when the satellite ascending through atmosphere. **Fig. (1)** shows the external satellite heat balance. The heat transfer between satellite components is by conduction and radiation, and from satellite to space is by radiation only, no conviction exists due to vacuum. Satellite thermal analysis is concerned with predicting the temperature of a satellite in known or assumed environment. The numerical thermal modeling method treats the satellite as a set of small isothermal panels connected by the conductances that relate heat transfer to temperature differences. The thermal energy equation is then applied to each panel with the differentials replaced by ratios of small but finite differences, while local heat dissipation and boundary exchanges are combined into a single heat generation term, this technique is called lumped system technique. In this discrete form, a set of simultaneous algebraic equations is obtained involving panel temperatures with coefficients that are known functions of thermophysical properties and temperature.

The problem was investigated in literatures with different approaches.(Masao, et al.1984) presented thermal network modeling to describe the heat balance of a spacecraft. (Krishnaprakas. 1998) used the lumped-parameter network formulation to obtain a set of coupled, nonlinear; first-order ordinary differential equations whose solution gave the temperature distribution of spacecraft. (Kim and Chang.1999) presented absorbed heat-flux method for ground simulation of on-orbit thermal environment of KOMPSAT satellite (Korea Multi-Purpose Satellite). (Awda and Petrovic.2000) studied octagonal shape plate under constant temperature boundary condition, using finite difference numerical technique to solve Lapels partial deferential equation. (Coyl, et al. 2001) presented Spartnik satellite thermal design, the Spartnik was octagonal body 30kg micro-satellite in circular low earth orbit. (Roos and Diner. 2002) described the orbital thermal analysis of a satellite with articulating solar panels.

The present work is the first in Iraq in this field. A thermal analysis of an earth orbiting octagonal shell body is developed. This body represents the payload of Iraqi satellite. The main objective was the development of a theoretical mathematical model to analyze the thermal behavior and performance of the body under different environmental conditions to calculate the transient and steady temperature distribution of the body. Besides, experimental test in a thermal vacuum chamber on a half-scale model of the original body prototype was made to investigate the problem.

MATHEMATICAL MODELING

The geometry, coordinate system and orientation of the problem is shown in **Fig. (2)**.The orbit of the body is circular with height (h) of (500 Km) and plane inclination angle (i) of (40°), see **Fig. (3)**. The orbit coordinate system is the earth centered inertial coordinate (ECI) coordinate system shown

in **Fig.(4)**, **Fig.(5)** shows the earth-sun- body system, the angular position of the body in its orbit relative to the earth-sun line is denoted by (η) the value of (η) at which the body enters the earth's shadow is given by (Kreith 1962) as;

$$\eta_{shadow} = \left(\frac{\sin\left(\sin\left(\cos^{-1}\left(\frac{Re}{r} \right) \right) \right)}{\sin(\tau)} \right) + 90 \quad (1)$$

$$r = Re + h \quad (2)$$

and the total included shadow angle (η_{throsh}) is;

$$\eta_{throsh} = 180 - (\eta_{shadow} - 90) * 2 \quad (3)$$

The time spent in the earth's shadow is;

$$t_{shadow} = \frac{\eta_{throsh} . \pi . r}{180 . V_S} \quad (4)$$

where;

$$V_S = \left(\frac{g . Re^2}{r} \right)^{1/2} \quad (5)$$

is the circular body velocity. The declination angle (δ) between solar vector and equatorial plane is calculated by (Beckman 1974) as;

$$\delta = 23.45 \sin\left(360 \frac{(284 + Nd)}{365} \right) \quad (6)$$

where (Nd) is the day number for the year period.
The thermal analysis of the body assumes that there is no temperature variation across the thickness of the octagonal shell body, the material properties and surface properties are independent of temperature, no radiation exchange between internal surfaces, surfaces are gray surfaces; properties are independent of the wavelength. The analysis is based on a simple lumped-capacity concept. The body is divided into segments that are small enough so that the temperature can be regarded as constant over the surface, and the outer normal is constant. The instantaneous heat balance on the n^{th} segment is given by:

$$q_{ern} + q_{irn} + q_{icn} + P_n = C_n \frac{dT_n}{dt} \quad (7)$$

where:
(q_{ern}) is the net radiation exchange with the environment.

(q_{irn}) is the net radiation exchange with other segments of the body.

(q_{icn}) is the net conduction exchange with other segments of the body.

(P_n) is the internal generation in the segment.

(C_n) is the thermal capacity of the segment.

(T_n) Is the temperature of the segment.

The net radiant exchange with the environment (q_{ern}) is calculates as;

$$q_{ern} = \alpha F_S S + \varepsilon F_e E + \alpha F_r f\ S - \varepsilon\sigma T_n^4 \qquad (8)$$

Where (Fs, F_e and F_r) are the sun, earth, and albedo shape factor, (f) is the albedo constant, (S) is the solar constant, and (E) is the earth radiation, and the radiation and conduction exchange with other segments are given by:

$$q_{irn} = \sum_m \Im_{mn} (\sigma T_m^4 - \sigma T_n^4) \qquad (9)$$

$$q_{icn} = \sum_m K_{mn} (T_m - T_n) \qquad (10)$$

Where ($\Im_{mn}$) is the shape factor between nodes (m and n) and (K_{mn}) is the conductance between nodes (m and n).

The solar constant (S) is closely approximated by (Beckman 1974) as;

$$S = 1353 * \left(1 + 0.033 * \cos\left(\frac{360 * Nd}{365}\right)\right) \qquad (11)$$

The calculations of the shape factor (Fs, Fe and Fr) are very complex because the body is moving around the earth. In the present work, they are calculated every (45°) interval in the orbit. They are calculated based on relations given by (Siegel and Howell 1972). The sun shape factor;

$$Fs = \cos\Phi \qquad (12)$$

where (Φ) is the angle between the solar vector and element normal vector. The earth shape factor for horizontal (F_{eH}) and vertical (F_{ev}) elements are respectively given by;

$$F_{eH} = 2\int_0^{\cos^{-1}\frac{1}{(1+\nu)}} \int_0^{2\pi} \frac{\sin\varphi\cos\varphi\left[1+(1+\nu)^2-2(1+\nu)\cos\varphi-\sin\varphi^2\right]^3}{\left[1+(1+\nu)^2-2(1+\nu)\cos\varphi\right]^2} \qquad (13)$$

$$\frac{-\sin\varphi\sqrt{1+(1+\nu)^2-2(1+\nu)\cos\varphi-\sin\varphi^2}}{} d\psi d\theta \frac{1}{\pi}$$

$$F_{c\text{-}V}=2\int_{0}^{\cos^{-1}\frac{1}{(1+\nu)}}\int_{0}^{2\pi}\frac{\sin\varphi^{2}\cos\varphi\sin\psi\sqrt{1+(1+\nu)^{2}-2(1+\nu)\cos\varphi-\sin\varphi^{3}}-\sin\varphi^{4}\sin\psi}{\left[1+(1+\nu)^{2}-2(1+\nu)\cos\varphi\right]^{2}}d\psi d\varphi-\frac{1}{\pi} \quad (14)$$

where (φ) and (ψ) are zenith and azimuth angles and ($\nu = a/R$) is the ratio of elevation to radius. The albedo shape factor (F_r) is calculated by using eq. (13) and eq. (14), except that the upper limit of the inner integrals is (ψ) instead of (2π), where

$$\psi = 360 - \left[\frac{360}{2.\varphi_{max}}\right].(\lambda - \varphi_{safety}) \quad (15)$$

where

$$\varphi_{safety} = \frac{\pi}{2} - \varphi_{max} \quad (16)$$

$$\xi = 2.\varphi_{max} + \varphi_{safety} \quad (17)$$

the integration here is divided into three regions, the first one is when ($\lambda \leq \varphi_{sefety}$), the second is when ($\varphi_{sefety} < \lambda < \xi$) and the third is when ($\lambda \geq \xi$), see **Fig. (6)**.

NUMERICAL FORMULATION

A numerical calculation algorithm has been developed to solve the governing equations of the mathematical model described in the previous article. A finite difference control volume approach with explicit scheme method has been adapted. The grid of **Fig. (7)** is generated at first. The node is identified by the indices (i, j). The nodes on the edges of the octagonal body where the two side panels intersect have boundary conditions from the two panels. It can easily be shown that eq. (7) can be written as;

$$T_n^{t+\Delta t} = \left[\ \alpha Fs\, S\, A_n + \varepsilon Fe\, E\, A_n + \alpha Fr\, f\, S\, A_n + \sum_m K_{mn}\,(T_m - T_n) + P_n - \varepsilon\sigma A_n T_n^4\ \right]^t \frac{\Delta t}{C_n} + T_n^t \quad (18)$$

where:

$$K_{mn} = \frac{kA_{mn}}{r_{mn}} \quad (19)$$

and

$$Cn = \rho cp v_n \quad (20)$$

The developed computational algorithm was converted to a computer program in FORTRAN 90 whose main output is the transient and steady temperature distribution of the body and the heat fluxes on its faces at different environment as conditions.

EXPERIMENTAL TESTS

The experiments conducted in the present work were made to test a half-scale model of the original prototype in a thermal vacuum chamber. The model was manufactured from aluminum sheet type (2024-T36). During the test, the model was covered with silver wrapper. The model was instrumented with (14) thermal Resistance type (PT-100). The thermal vacuum chamber is a cylindrical container (1.5 m) in diameter and (1.5 m) length, both ends are of dish type ended, one is fixed and the other is movable to handle the tested model inside the chamber, see **Fig. (8)** and **Fig. (9)**.

RESULTS AND DISCUSSIONS

The grid size of the computational domain was optimized to 336 nodes according to **Fig. (10)**. The heat fluxes on the body faces against orbital position (ω) was studied, for three different inclination angles ($i=30^{\circ}$, $40^{\circ}$and 50°) for three orbit heights (h=400,500 and 600 Km) and for four days in the year (vernal equinox, summer solstice, autumnal equinox and winter solstice). Samples are shown in **Figs. (11)** to **(14)**. It is clear that the heat fluxes are maximum in winter solstice and minimum in summer solstice. The albedo and earth heat fluxes effects decrease with orbital height increase. The light region increases with increasing orbit height. In the side faces the heat fluxes are maximum when orbit inclination is minimum, and vice versa the inverse behavior is true for the upper and lower faces. The temperature variations with time of selected nodes on the body faces are studied. Samples are shown in **Fig. (15)** and **Fig. (16)** for summer and winter solstice days, respectively. In **Fig. (15)**, the absorptivity is three times the emissivity, therefore the nodes are heated, the nodes reach to synchronous steady state after 9 orbits, where the orbit time is (94.5) minutes because the difference between the emissivity and absorptivity is high. The worst hot temperature is (146.4°C) at node (4) and the worst cold temperature is (113.5°C) at node (1). In **Fig. (16)**, the emissivity is higher, and therefor the nodes are cooling, and they reach the synchronous steady state after 2 orbits because the difference is low. The hottest temperature is (60.2 $^{\circ}$C) and the coldest is (-39 $^{\circ}$C). The temperature difference between the nodes on the body is large when the absorptivity is large. The average temperature of the body faces were calculated and plotted for different condition. **Fig. (17)** and **Fig. (18)** are samples at summer and winter solstice days respectively. The behavior of the average temperature is the same as that of nodes on the same face, with different values. **Fig. (19)** shows a comparison between the theoretical and experimental results of the present work. The agreement is good, with about (5%) average error. The main cause of this error is the neglecting of the thermal contact resistance in the theoretical model.

CONCLUSIONS

A theoretical and experimental investigation of the thermal behavior of an octagonal shell earth orbiting body has been made in the present work. It was found that the heat fluxes on the body faces are maximum in winter solstice and minimum in summer solstice. These fluxes are inversely proportional to the orbit inclination in the side faces of the body. The inverse is true for the upper and lower faces. The body reaches the synchronous steady state temperature faster when the difference between the emissivity and absorptivity is low. The emissivity effect is larger than that of absorptivity. The temperature of the sides facing the earth fluctuates more than the other faces.

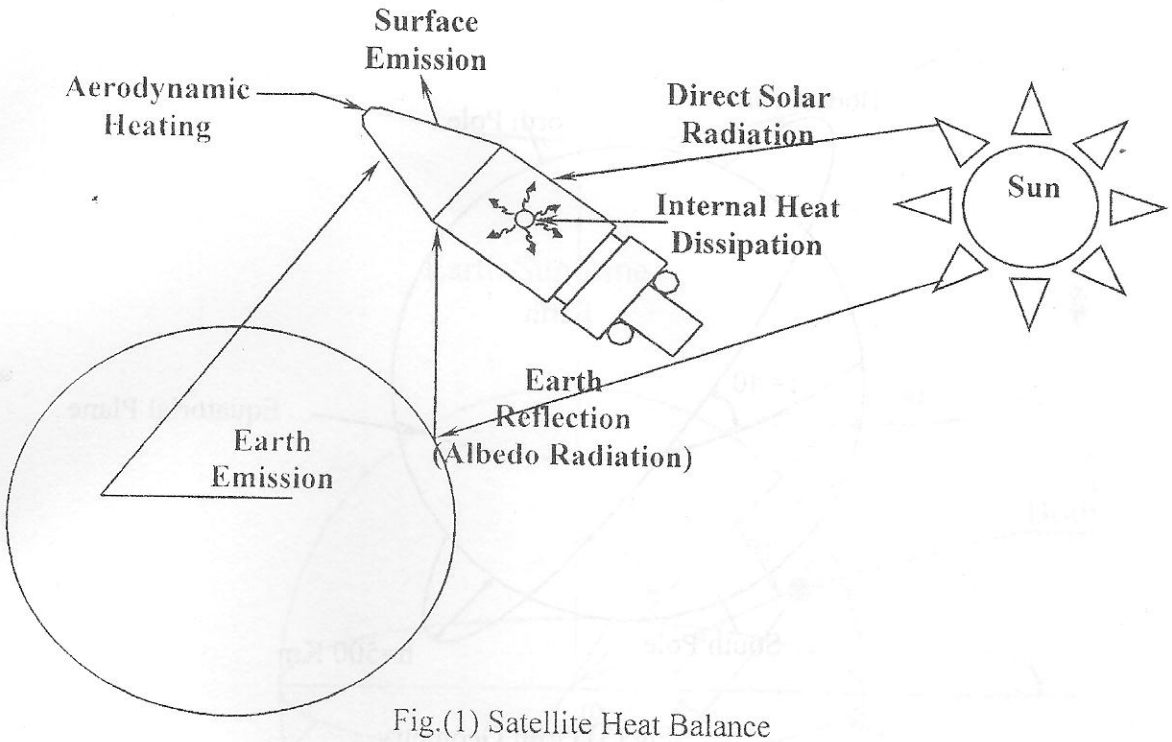

Fig.(1) Satellite Heat Balance

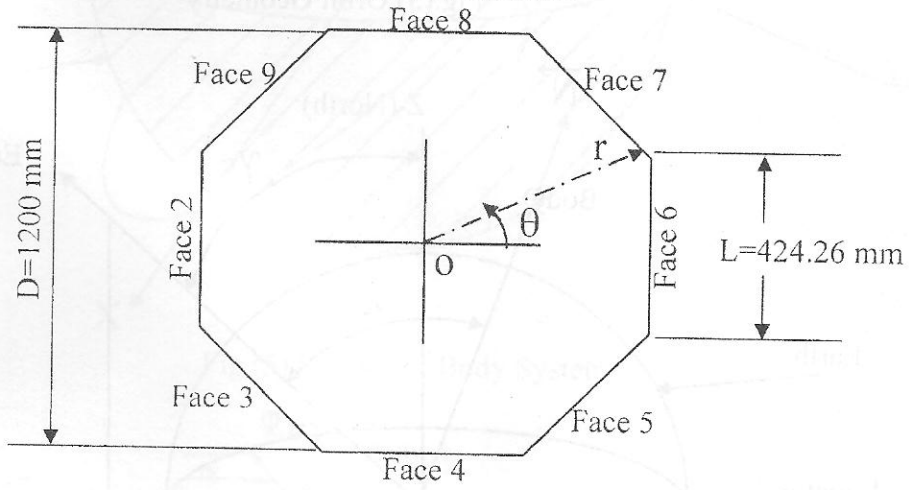

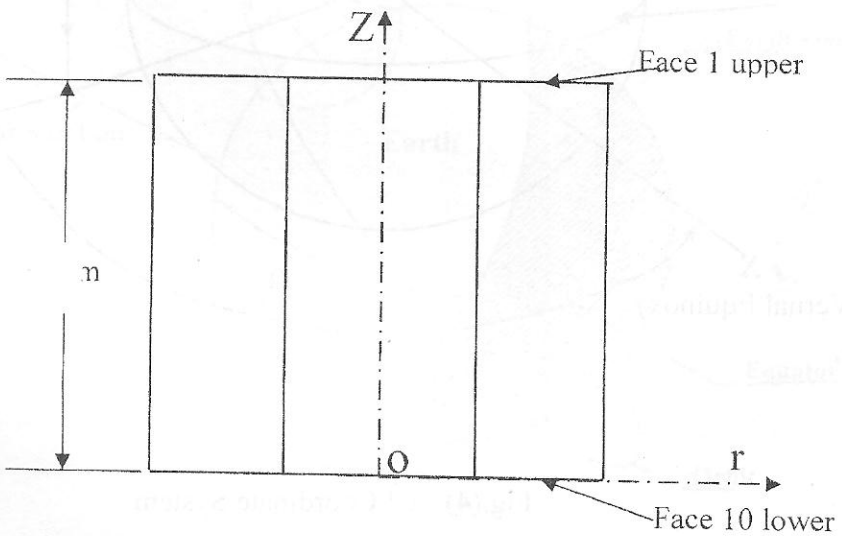

Fig.2: Orbiting Body Coordinate System and Orientation

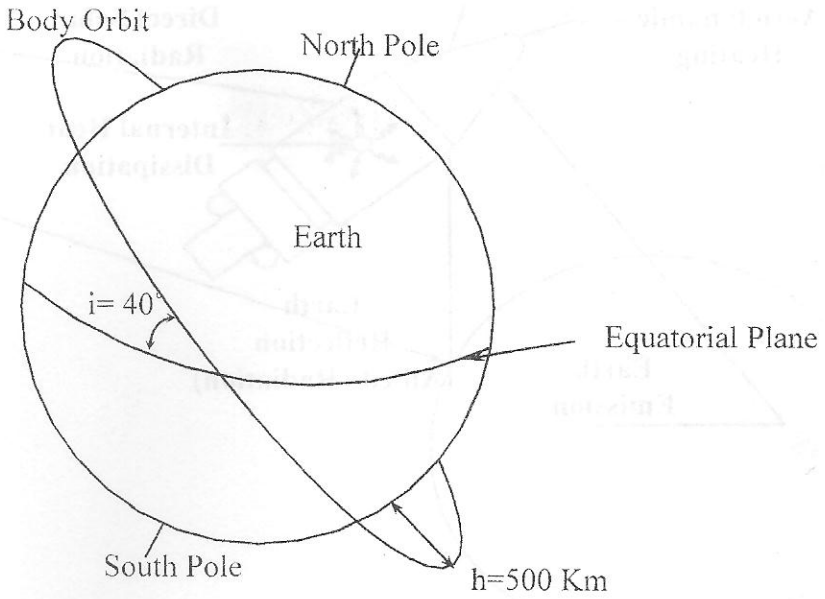

Fig.(3) Orbit Geometry

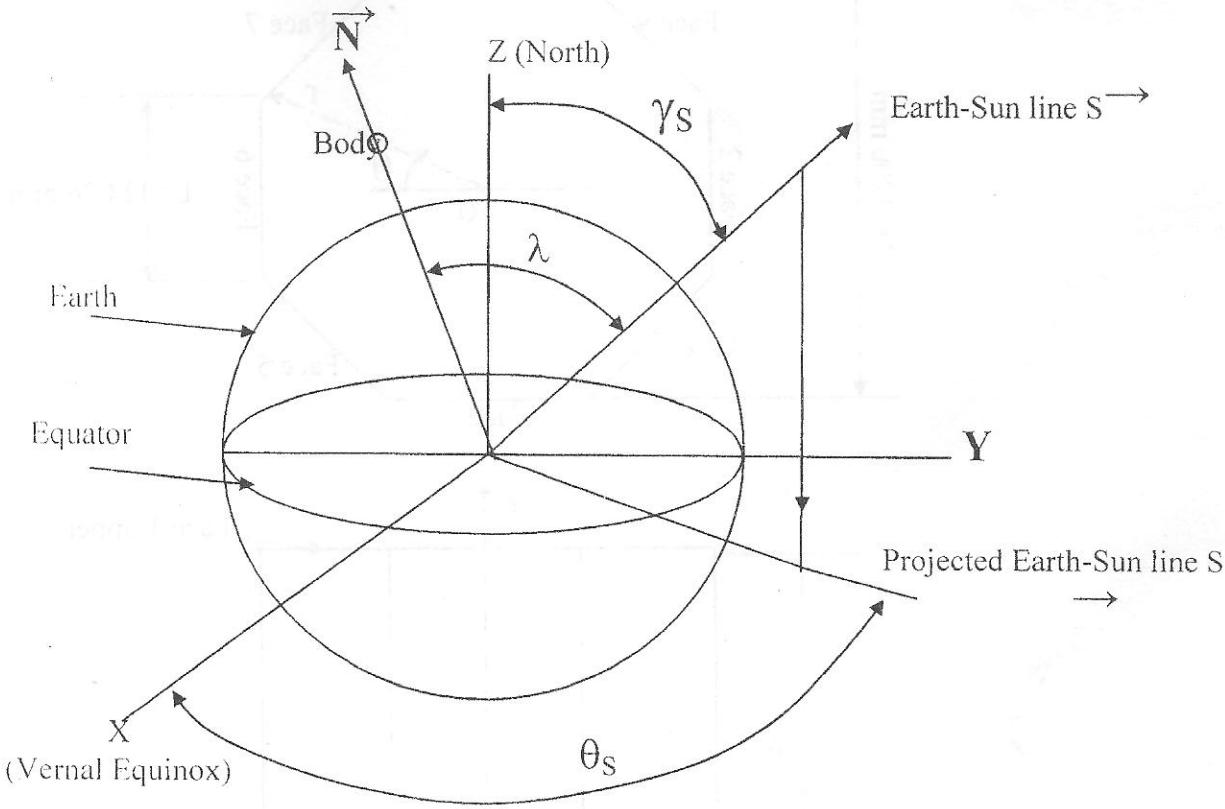

Fig.(4) ECI Coordinate System

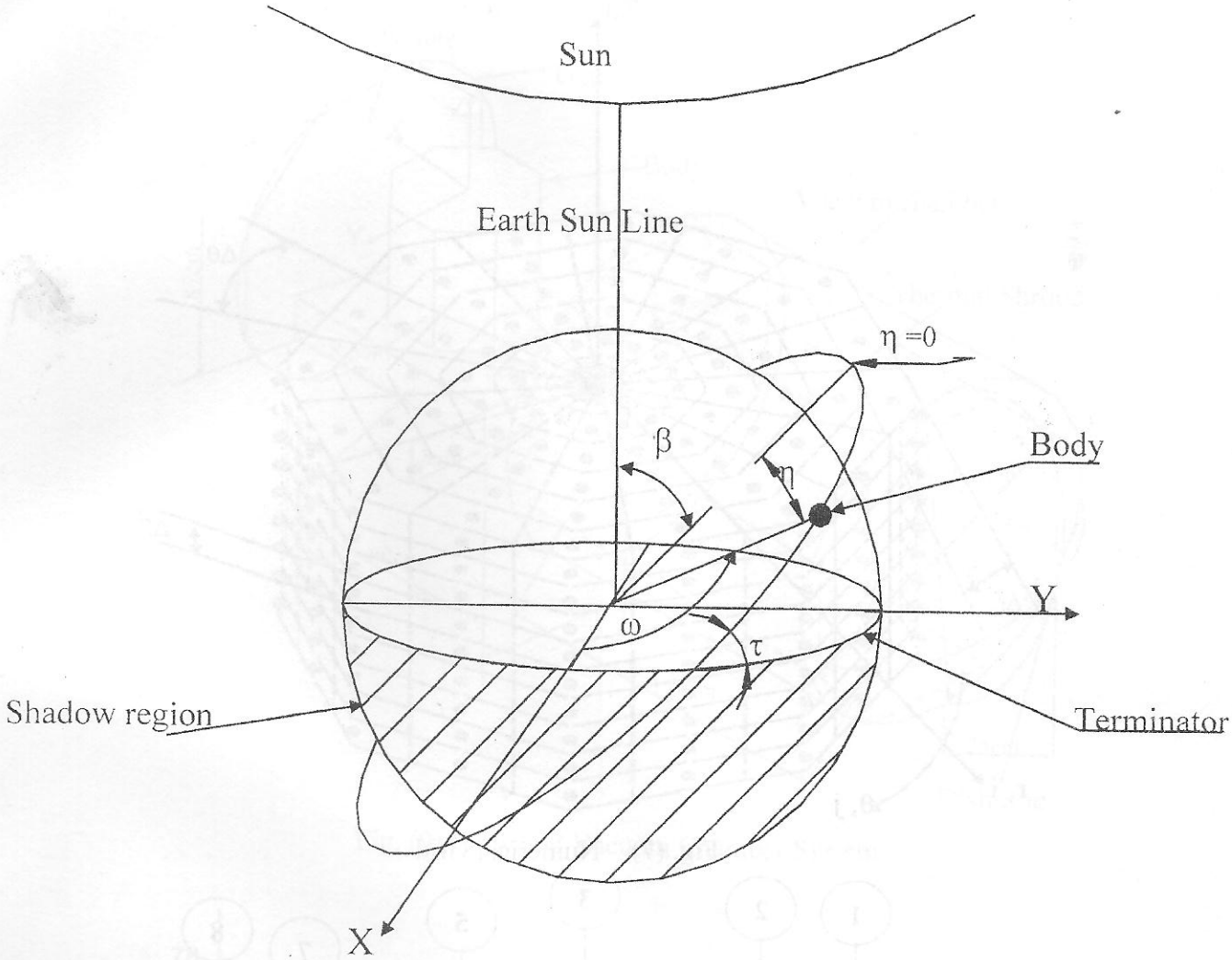

Fig.(5) Earth-Sun-Body System

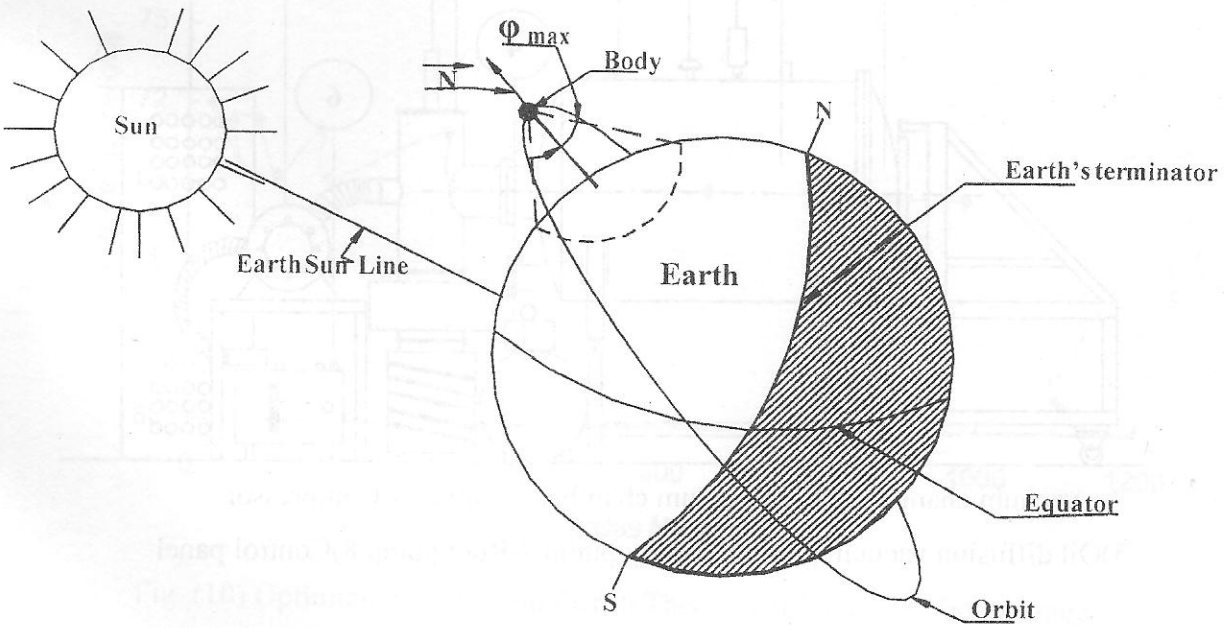

Fig.(6) Earth-Sun-Body System and Solid Angle (φ_{max})

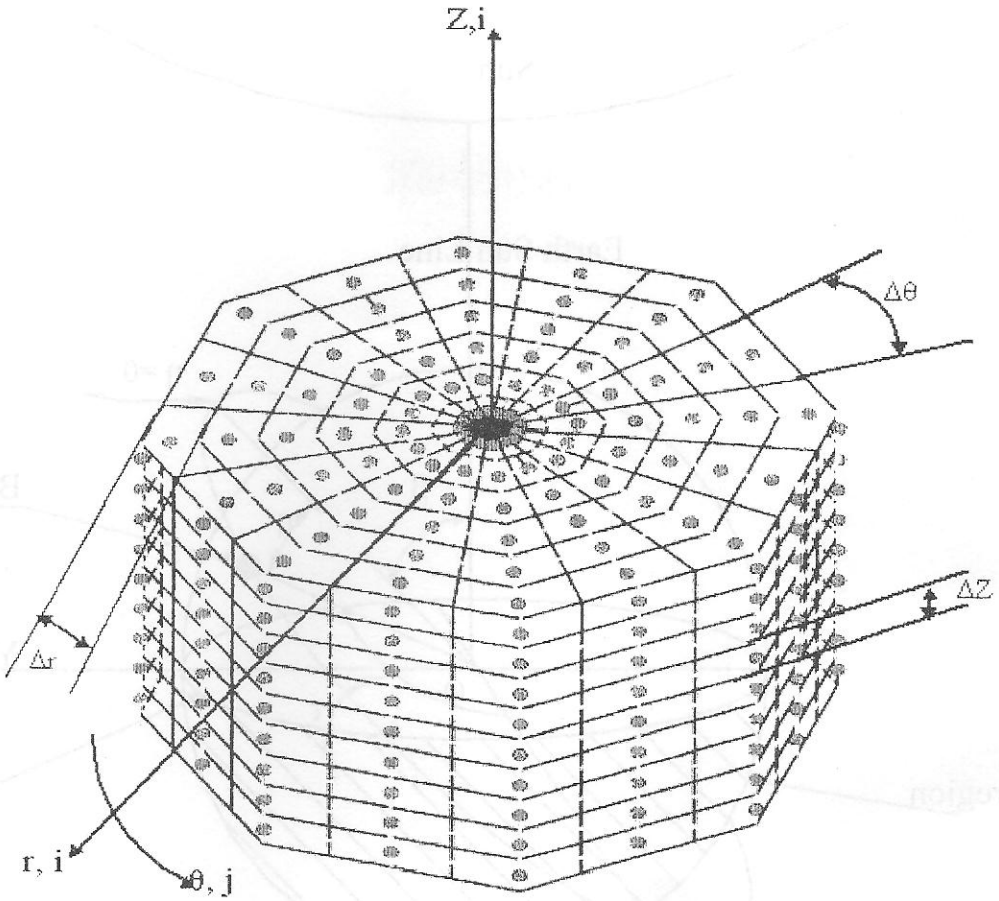

Fig. (7) Numerical Grid

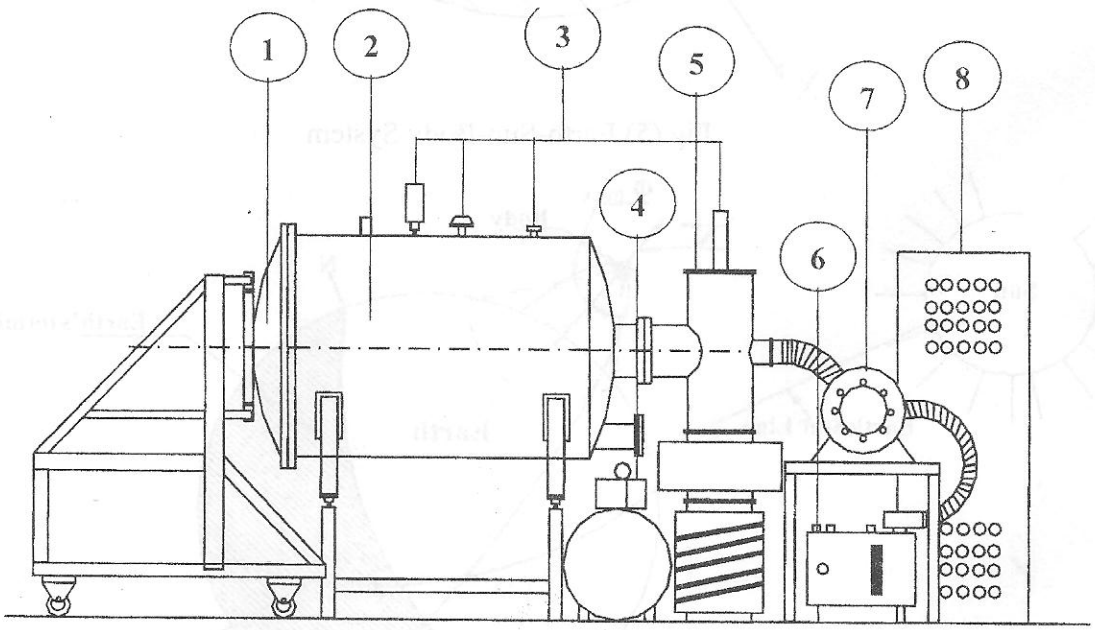

vacuum chamber gate 2)Vacuum chamber 3)Valves 4)Compressor
5)Oil diffusion vacuum pump 6)Rotary pump 7)Root pump 8)Control panel

Fig. (8) Vacuum Chamber External Parts

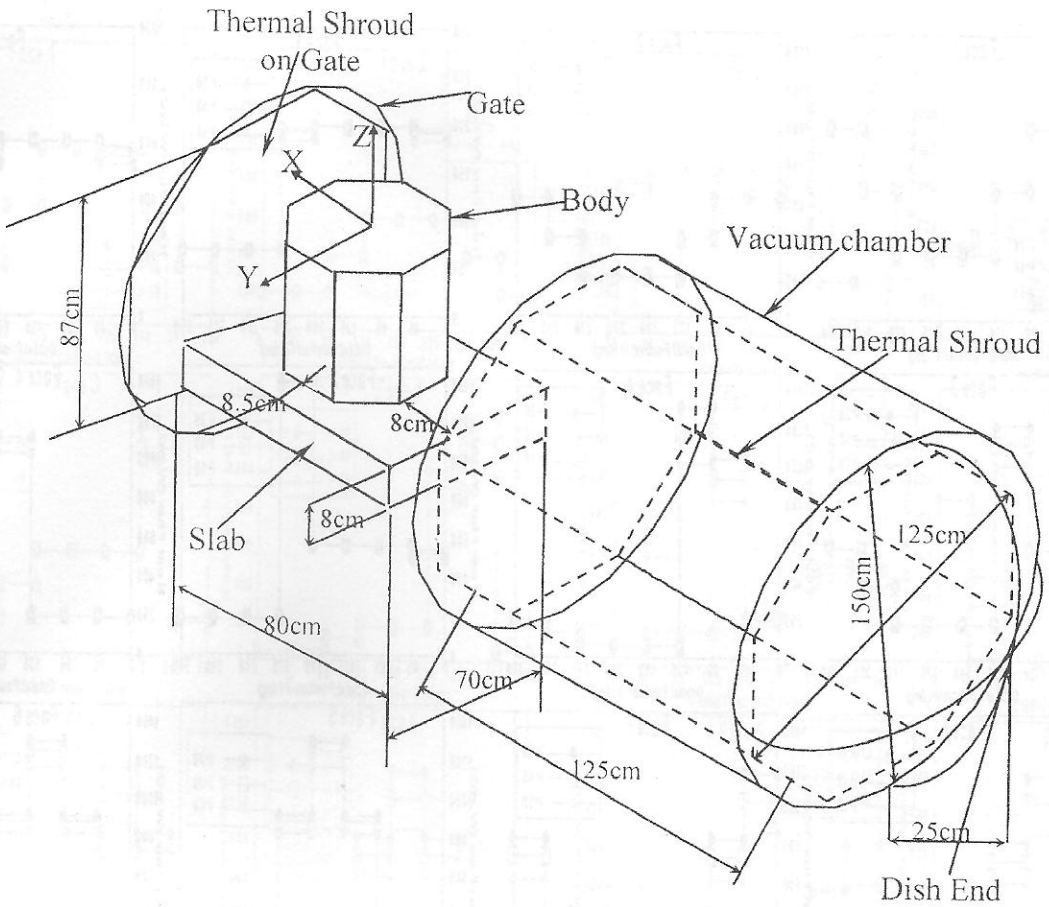

Fig. (9) Body and Vacuum Chamber System

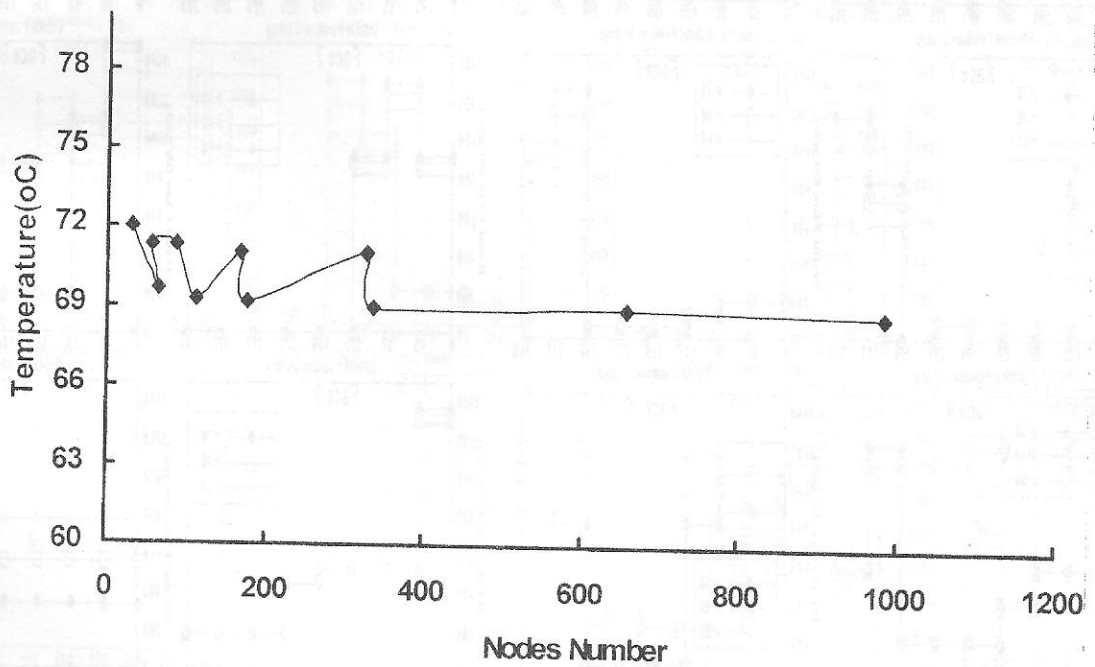

Fig. (10) Optimizing Nodes Number in Theoretical Model for the Average Temperature at Last Column

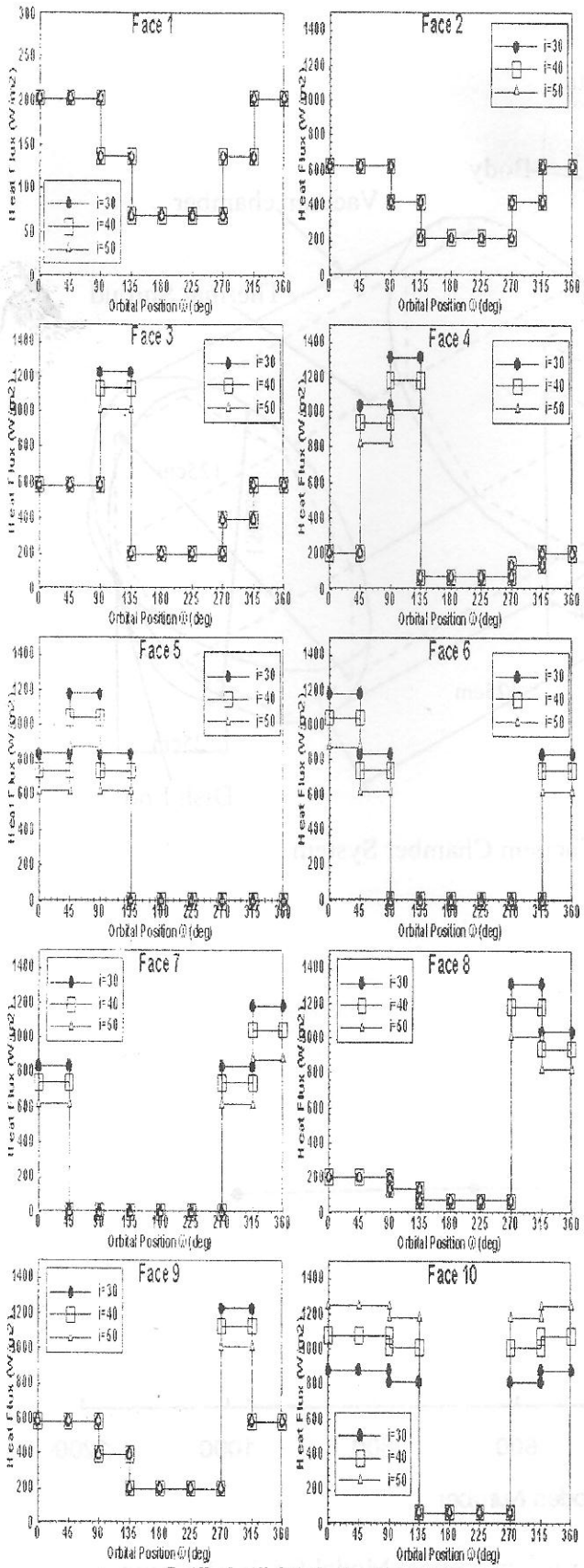

Fig. 11 Total Heat Load Vs Orbital Position, orbit height 400Km at Vernal Equinox

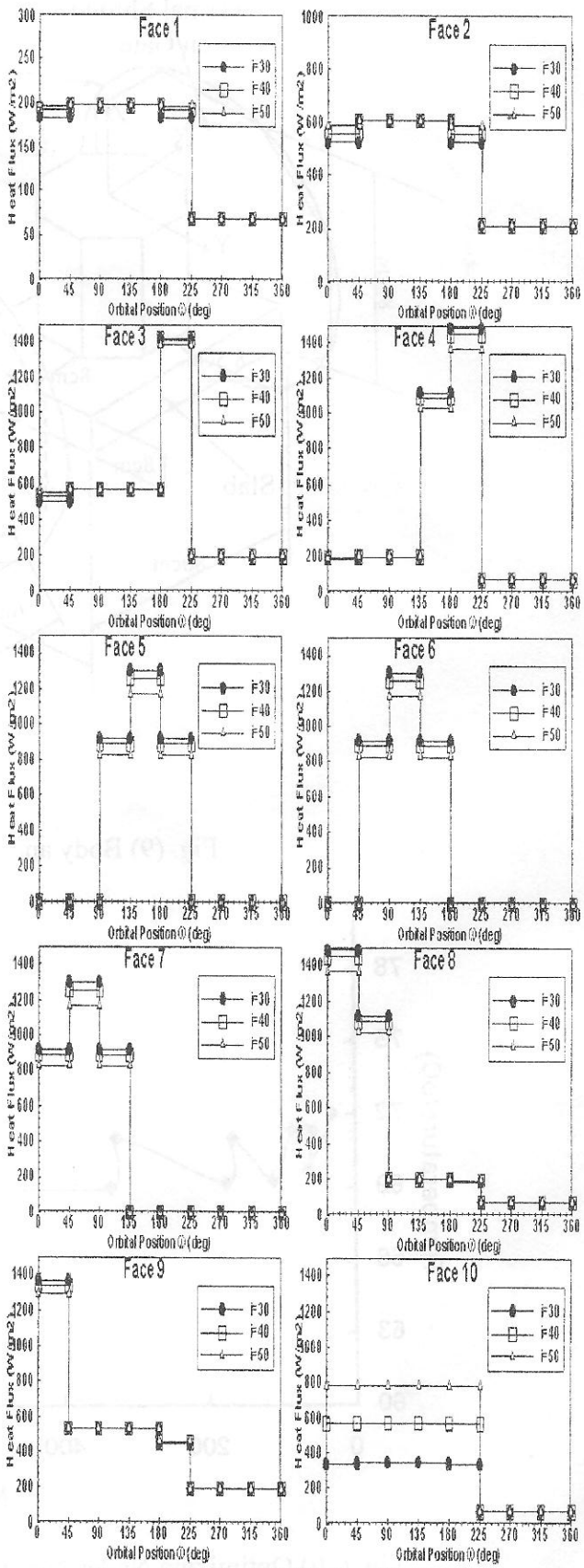

Fig. 12 Total Heat Load Vs Orbital Position, orbit height 400Km at Summer Solstice

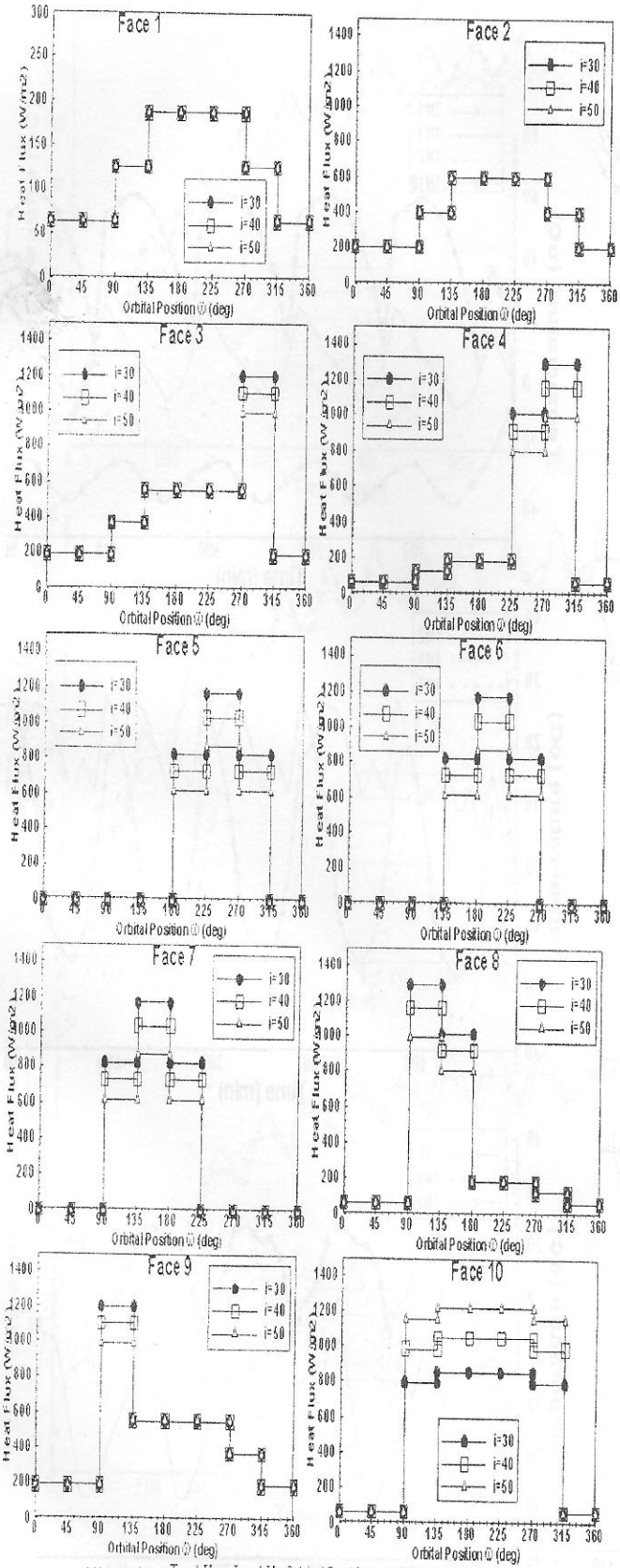

Fig 13 Total Heat Load Vs Orbital Position, orbit height 500Km at Autumnal Equinox

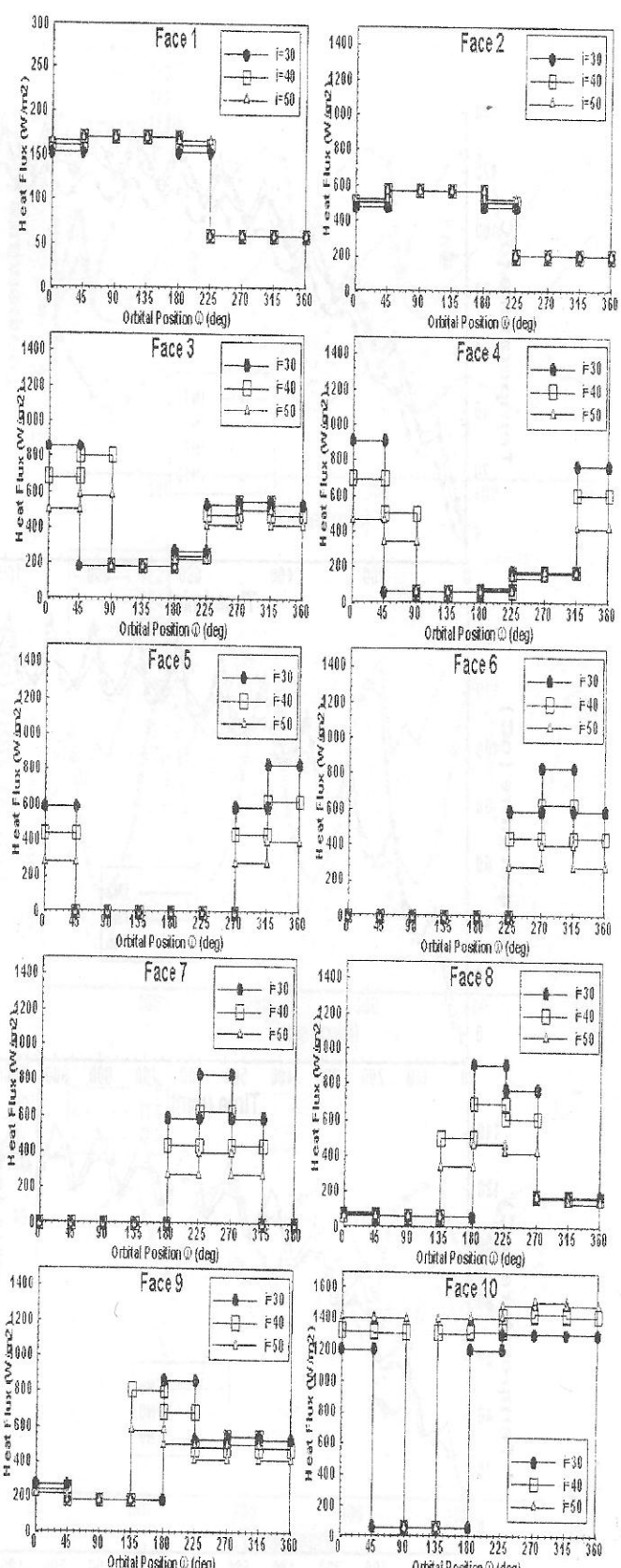

Fig 14 Total Heat Load Vs Orbital Position, orbit height 600Km at Winter Solstice

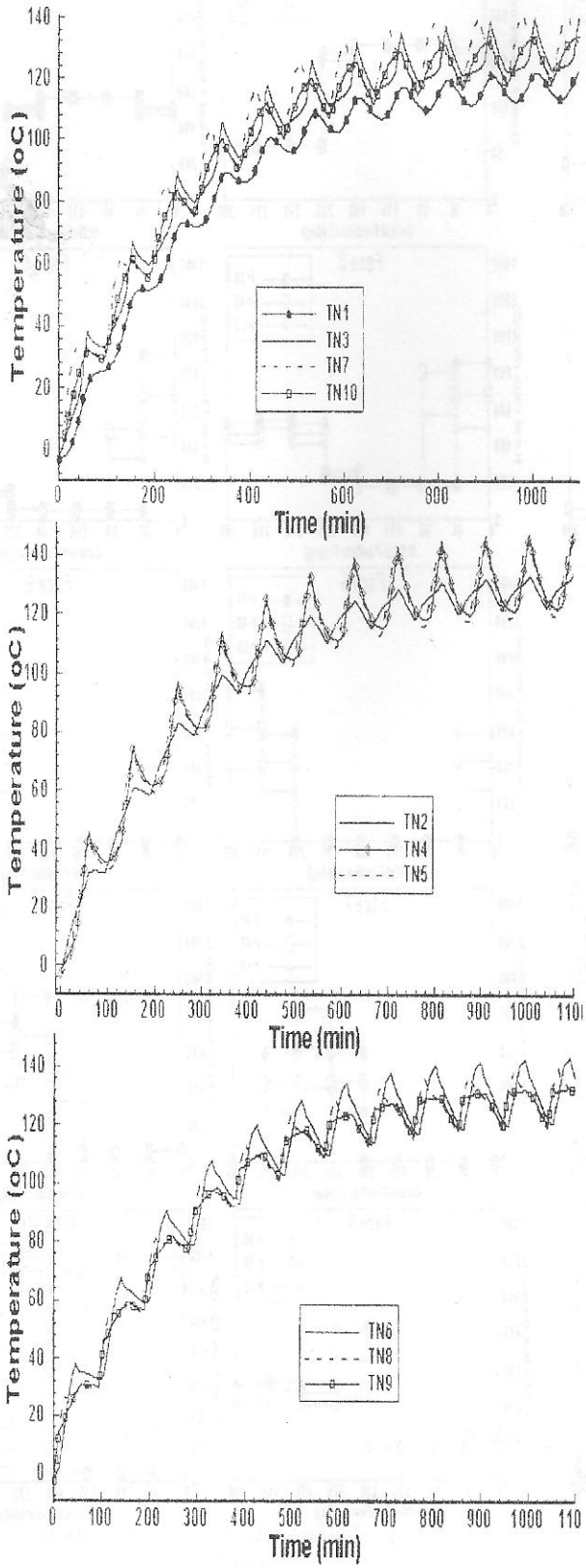

Fig. 1 Temperature of Selected Nodes on Body Against Time at α=0.2 and ε=0.05 (Polished Aluminum)

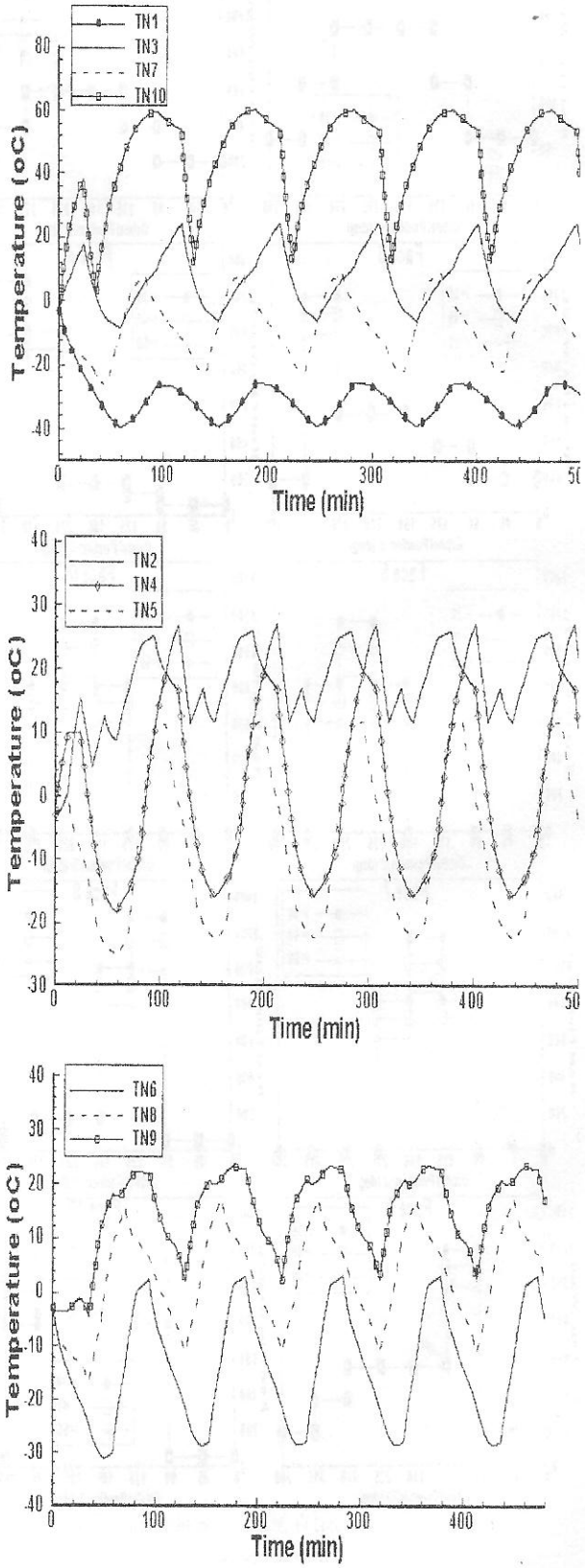

Fig. 1 Temperature of Selected Nodes on Body Against Time at α=0.583 and ε=0.87 (AL+Kapton)

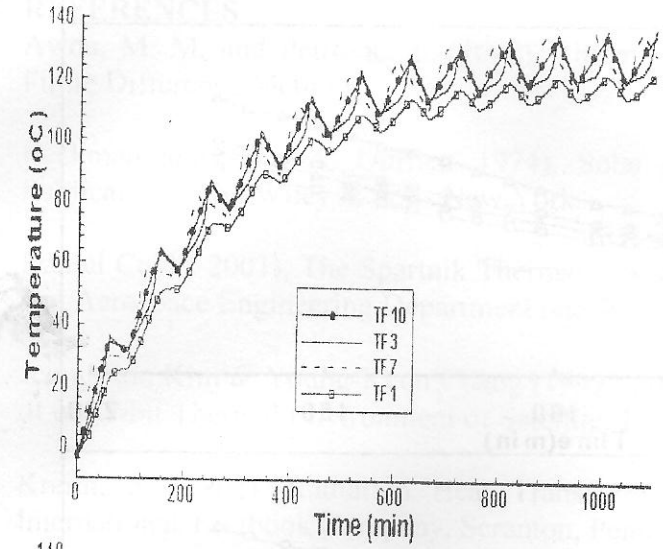

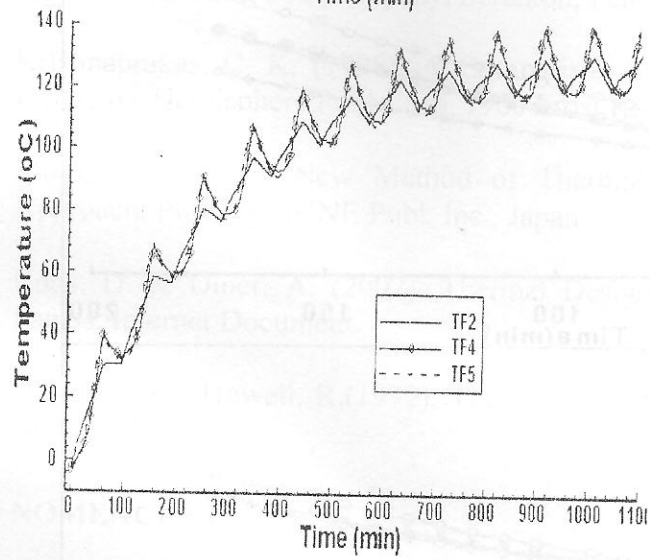

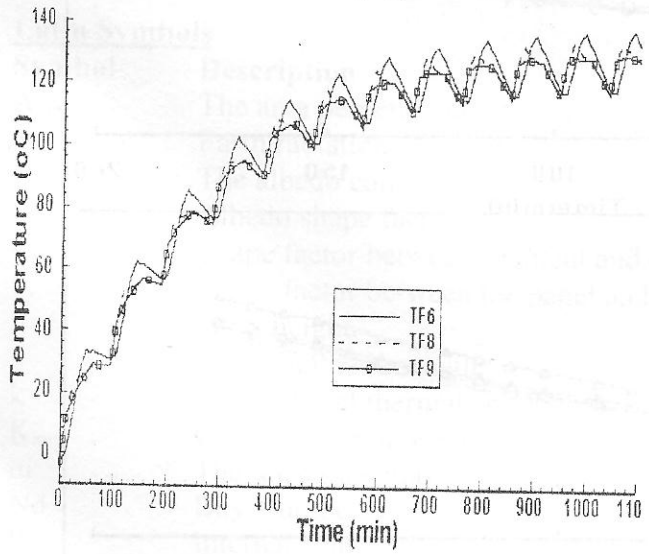

Fig.17 Average Temperature on Body Faces Against Time at α=0.2 and ε=0.05 (Polished Aluminum)

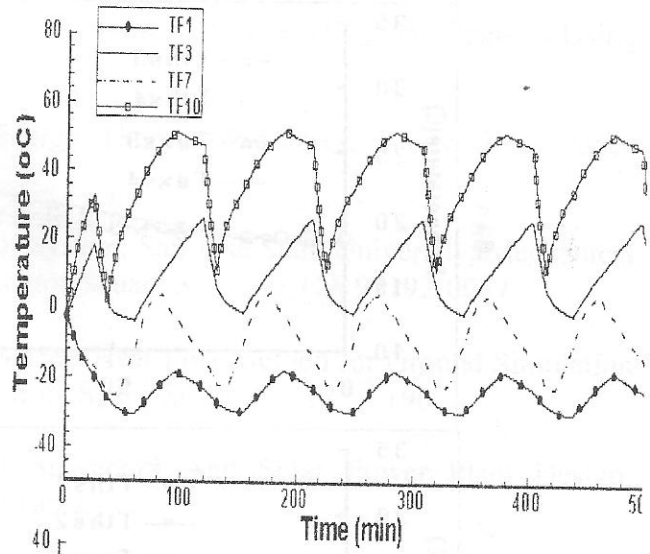

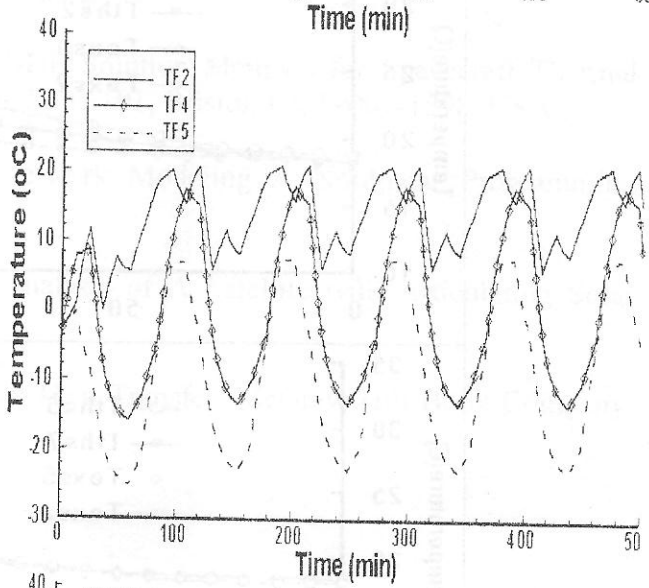

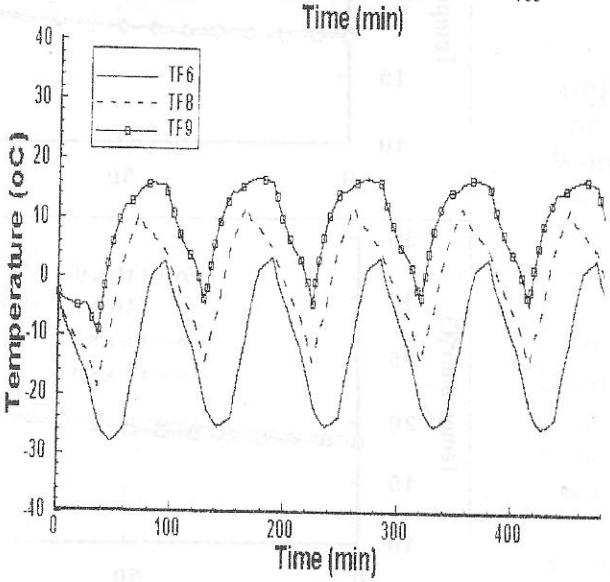

Fig.18 Average Temperature on Body Faces Against Time at α=0.583 and ε=0.87 (Al+Kapton)

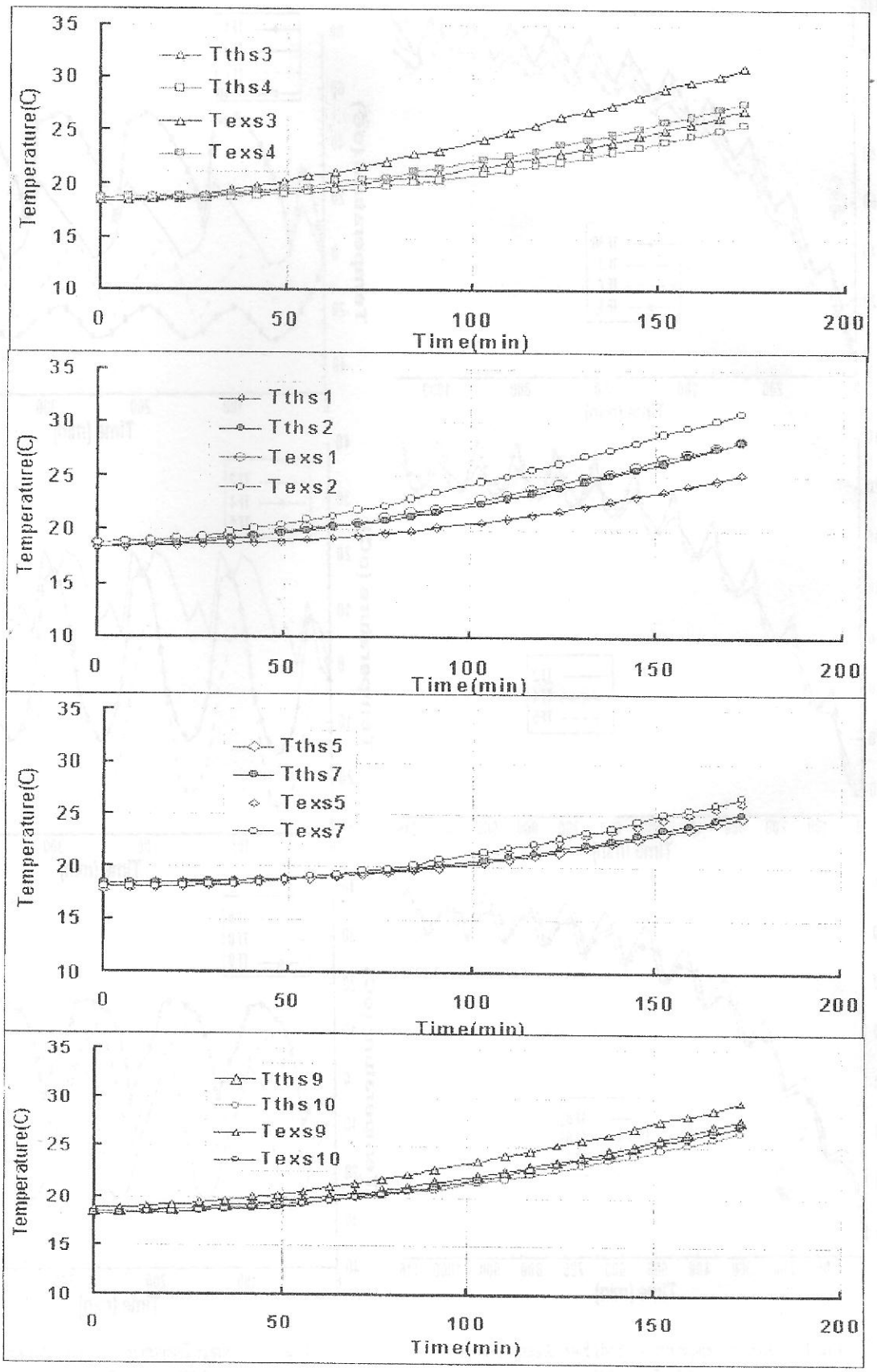

Fig. 19: Comparison between Theoretical and Experimental Results

REFERENCES

Awda, M. M. and Petrovic, Z. (2000), Thermal Distribution of Non Rectangular Regions Using Finite Difference Method.

Beckman and John A. Duffie,(1974), Solar Energy Thermal Processes, Wiley- Interscience Publication, John Wiley & Sons New York.

Daniel Coyl (2001), The Spartnik Thermal Control System, San Jose State University, Mechanical and Aerospace Engineering Department one Washington square San Jose, CA 95192-0087.

Jeong-Soo Kim & Young-Keun Chang (1999), Absorbed Heat-Flux Method for Ground Simulation of on-Orbit Thermal Environment of Satellite, J. Astron. Space Sci. 16(2), 177 _ 190.

Kreith, F. (1962), Radiation Heat Transfer For Spacecraft And Solar Power Plant Design, International Textbook Company, Scranton, Pennsylvania.

Krishnaprakas, C. K. (1998), A Comparison of ODE Solution Methods for Spacecraft Thermal Problems, Hemisphere Publ Corp, 1900 Frost Road, Suite 101, Bristol, PA 19007-1598, USA.

Mosao ,A.(1984), New Method of Thermal Network Modeling A Nonlinear Programming Approach, Publ. by AGNE Publ. Inc., Japan.

Roos, D. & Diner, A. (2002), Thermal Design Analysis of A Satellite with Articulating Solar Panels, Internet Document.

Siegel R. and Howell, R.(1972), Thermal Radiation Heat Transfer, McGraw-Hill Book Company, New York.

NOMENCLATURE

Latin Symbols

Symbol	Description	Unit
A_{mn}	The area perpendicular to r_{mn}.	m^2
E	Earth radiation constant.	W/m^2
f	The albedo constant.	—
F_r	Albedo shape factor.	—
F_e	Shape factor between segment and earth.	—
F_s	Shape factor between the panel and sun.	—
h	Orbit height.	Km
i	Orbit inclination angle.	Degree
k	The material thermal conductivity.	W/m K
K_{mn}	Conductance between nodes (m and n).	W/m K
m	The specimen mass.	Kg
Nd	Day Number.	—
P_n	Internal heat generation in the segment.	W/m^3
q_{ern}	Net radiation exchange with the environment.	W/m^2
q_{irn}	Net radiation exchange with other segments of the body.	W/m^2
q_{icn}	Net conduction exchange with other segments of the body.	W/m^2
r_{mn}	Distance from the earth center to the orbit.	Km

Re	Earth radius.	Km
S	The solar constant.	W/m^2
t	Time .	s
t_{shadow}	Time spent in the earth's shadow.	s
T	Temperature.	K
Vs	Circular body velocity.	m/s^2
v_n	Volume of control volume contains the node.	m^3

GREEK SYMBOLS

Symbol	Description	Unit
α	The thermal absorptivity.	—
β	Angle the solar vector makes with orbit plane.	Degree
δ	The declination angle.	Degree
ε	The total hemispherical emissivity.	—
Φ	The angle between the solar vector and element normal.	Degree
γ_S, θ_S	Position angles to the solar vector.	Degree
η	Orbit position to body in orbit with relative to noon.	Degree
φ	Zenith angle on the sphere's surface.	Degree
φ_{max}	Maximum solid angle view to the sphere.	Degree
λ	The angle between body normal vector and sun vector.	Degree
ρ	The material density.	Kg/m^3
σ	The Stefan Boltzmann constant.	W/m^2K^4
ω	Angular position in orbit with relative to X- axis.	Degree
ψ	Azimuth angle on the sphere's surface.	Degree

SUBSCRIPTS

Symbol	Description
m	m^{th} segment.
n	n^{th} segment.

SUPERSCRIPTS

Symbol	Description
t	At time t
$t+\Delta t$	After time Δt